ISSN: 0067-2904

Influence of Magnetic Force for Peristaltic Transport of Non-Newtonian Fluid Through Porous Medium in Asymmetric Channel

Amaal Mohi Nassief*, Ahmed M. Abdulhadi
Department of Mathematics, College of Science, University of Baghdad, Baghdad, Iraq

Received: 8/8/2022 Accepted: 23/10/2022 Published: 30/7/2023

Abstract:
In this paper, we study the effects of a magnetic force on the flow of hybrid bio - nano fluid (Cu - Au. NPs) for a peristaltic channel through a porous medium in an asymmetric channel. Nanoparticles of gold and copper as well as the blood (the base fluid) is taken into account. By using the Adomian decomposition method to solve the governing equations, formulas for velocity, stream function, temperature, current density, and magnetic force have been obtained. The findings show that Gold nanoparticles have an elevation magnetic force compared with copper nanoparticles, based on fluid (blood) and hybrid nanofluid. Finally, the phenomenon of trapping is offered as an explanation for the physical behavior of many parameters. The effect of physical parameters is plotted and analyzed by using the Mathematica software.

Keywords: Porous medium, Adomain decomposition technique, Peristaltic transport, Magnetic force, Current density.

تاثير القوة المغناطيسية للنقل التمعجي لمائع لانيوتيني بوسط مسامي في قناة غير متماثلة

امال محي نصيف*,احمد مولود عبد الهادي
قسم الرياضيات , كلية العلوم , جامعة بغداد , بغداد, العراق

الخلاصة :
في هذا البحث درسنا تاثيرالقوة المغناطيسية للنقل التمعجي للسائل النانوي الهجين عبر وسط مسامي في قناة غير متماثلة, يعتبر الدم سائلا اساسيا والذهب والنحاس جزيئات نانونية. استخدمنا طريقة (Adomain decomposition)لحل المعادلات الحاكمة, تم الحصول على, السرعة, دالة الجريان, درجة الحرارة, كثافة التيار والقوة المغناطيسية. تظهر النتائج ان جسيمات الذهب النانونية لها قوة مغناطيسية مرتفعة مقارنة بجسيمات النحاس النانوية، والسائل الاساسي (الدم) والسائل النانوي الهجين. اخيرا, وضحت ظاهرة التكوين السلوك الفيزيائي لعدة معلمات فيزيائية. وتم رسم تاثير المعلمات الفيزيائية وتحليلها باستخدام برنامج Mathematica .

1- Introduction:

Many researchers and engineers have given significant interest in nanofluids (NF) because it is used in a variety of biochemical and medical industries. Nanofluids are colloidal nanoparticle suspensions (NPS) in a base fluid, which was first reported by Choi[1]. Several nanoparticles such as Gold, silver and copper particles are used in proteins, administering drugs, and nucleic acids due to the great biocompatibility, magnetic, chemical, special mechanical,

*Email: amaal.mohi15@gmail.com

and thermal effects that these nanoparticles display. Gold nanoparticles are useful in cancer therapy because they are tiny and can penetrate the entire body, or due to their concentration at tumor sites due to permeability. Copper has strong antibacterial properties that are helpful in treating epidemic diseases. It has antibacterial and antifungal properties [2-4]. Because of the distinctive characteristics of gold and copper NPs are significantly important in biomedical science. The propagation of waves along the channel walls produces an important mechanism known as peristalsis. The peristaltic pumping of a nanofluid is an essential role in transportation for many biological and industrial procedures [5-8]. Many researchers attempted to investigate the peristaltic flows under the suspension of nanoparticles in light of the aforementioned uses. Kothandapani and Prakash [9] studied the impacts of thermal radiation and the heat source/ absorption parameters with the peristaltic flow of a hyperbolic tangent nanofluid model in the influence of n inclined magnetic field. Noreen et al.[10] discussed the effect of nanoparticles on the motion of blood in a vertical channel. Rashid et al. [11] investigated the Williamson fluid with induced magnetic field effects Hu et al.[12]examined the peristaltic flow through an asymmetric inclined channel when an external applied magnetic field without using the presumptions of lubrication theory. Zhang et al.[13]discussed entropy study of blood flow propagating through an anisotropic ally tapered artery under the suspension of magnetic Zane - oxide nanoparticles. Murad and Abdulhadi[14] discussed how a dilating peristaltic wave affects the peristaltic transport of a power-law fluid in an elastic tapered tube with varying cross sections. Seikh et al.[15] investigated that a uniform magnetic field and nanoparticles affect slip blood flow in combination. Kareem and Abdulhadi [16] investigated how varying viscosity, mass transfer, and heat transfer affect magneto hydrodynamic (MHD) peristaltic flow in an asymmetric tapering inclined channel through a porous medium.

Das et al.[17]studied the dual impacts of Hall and ion - slip currents through the peristaltic transport of a water-based nanofluid. Abo-Elkhair et al.[18]examined the thermal radiation and magnetic force on nanofluid via a peristaltic channel with a moderate Reynolds number. In an asymmetric channel with an applied magnetic field present. In addition, there are a lot of researchers who studied heat source\ sink in temperature gradient with porous medium [19-24]. A mathematical model is proposed to investigate the effects of the magnetic force on the peristaltic transport of hybrid bio-nanofluid (Cu - Au NPs) through an asymmetric channel with porous medium in light of the aforementioned research. The exact expressions of magnetic force, current density, temperature, stream function, and velocity. Graphs are used to illustrate how physical characteristics affect the flow, with the use of the Adomian decomposition technique.

2-Mathematical formulation:

A two dimensional incompressible and electrically conducting nanofluids have been taken into consideration through a porous medium in an asymmetric channel. The channel width is $d_0 + d_1$ and the wave moves in an X- axis at a constant speed of C. The rectangular coordinate system X, Y is specified with X-axis aligned with the channel's centerline and Y-axis aligned with the channel's transverse direction, as shown in (Figure (1)). The external magnetic field of strength h_0 is applied to the system, resulting in an induced magnetic field $\mathrm{H}(\mathrm{h}_x(\mathrm{x},\mathrm{y},\mathrm{t}), \mathrm{h}_y(\mathrm{x},\mathrm{y},\mathrm{t}) + \mathrm{h}_0, 0)$, which produces an induced magnetic field H the plate of channel walls, the upper wall $h_1$and the lower wall h_2 are represented by the peristaltic waves as

$$h_1(X,t) = d_0 + a_1 \cos\left[\frac{2\pi}{\lambda}(X - Ct)\right]$$
$$h_2(X,t) = d_1 + b_1 \cos\left[\frac{2\pi}{\lambda}(X - Ct) + \vartheta^*\right] \quad (1)$$

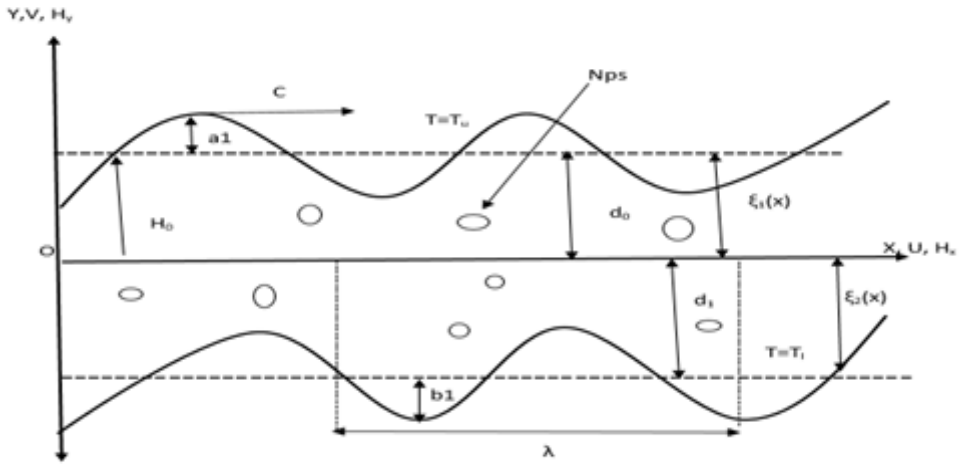

Figure 1: Geometry of problem

Where λ is the wave length, a_1, b_1 are the amplitudes of waves, ϑ^*represents the phase difference ($0 \le \vartheta^* \le \pi$), $\vartheta^* = 0$ is similar to a symmetric channel without phase waves, $\vartheta^* = \pi$ represents the waves are in phase, Moreover, $a_1 , d_1,\ d_0, b_1 , d_0$ and ϑ^*satisfy the condition $a_1^2 + b_1^2 + 2a_1 b_1 \cos\vartheta^* \le (d_0 + d_1)^2$.

The equations governing the problem are given by:

Maxwell's equation are:

$\nabla . \mathrm{E} = 0,\ \nabla . \mathrm{H} = 0,\ J = \nabla \times \mathrm{H}$

$\sigma[\mathrm{E} + \mu_e(\mathrm{V} \times \mathrm{H}^*)] = \mathrm{J}$

$$\nabla \times \mathrm{E} = -\mu_e \frac{\partial \mathrm{H}}{\partial \mathrm{t}} \tag{2}$$

Where E, J, σ, V and μ_e represent the electric field, current density, electrical conductivity, velocity vector and magnetic permeability.

The governing momentum, induction and heat equations of unsteady viscous incompressible nanofluid are given by[25].

$$\nabla . \mathrm{V} = 0 \tag{3}$$

$$\rho_{nf} \frac{\mathrm{DV}}{\mathrm{Dt}} = -\nabla \mathrm{P} + \mu_{nf} \nabla^2 \mathrm{V} + \mu_e (H^* . \nabla)\mathrm{H}^* - \mu_e \frac{\nabla \mathrm{H}^{*2}}{2} - \frac{\mu_{nf}}{\eta} \mathrm{V} \tag{4}$$

$$\frac{\partial \mathrm{H}^*}{\partial \mathrm{t}} = \nabla \times (\mathrm{V} \times \mathrm{H}^*) + \frac{1}{v^*} \nabla^2 \mathrm{H}^* \tag{5}$$

$$(\rho c_p)_{nf} \frac{\mathrm{DT}}{\mathrm{Dt}} = k_{nf} \nabla^2 \mathrm{T} + \mu_{nf} (\nabla \mathrm{V} + (\nabla \mathrm{V})^{\mathrm{T}})^2 - \frac{\partial \mathrm{q}}{\partial \mathrm{Y}} + \mathrm{Q}_0 \tag{6}$$

Where $\frac{\mathrm{D}}{\mathrm{Dt}}$ represents the total derivative, P is fluid pressure, $v^* = \mu_e \sigma_{nf}$ represents the magnetic diffusivity, σ_{nf} is the electrical conductivity. T represents the temperature distribution, $\mathrm{q} = -\frac{4\sigma_f^*}{3k_f^*} \frac{\partial \mathrm{T}^4}{\partial \mathrm{Y}}$ is the radiative heat flux, k_f^* and σ_f^* mean absorption coefficient and Stefan Boltzmann constants, Q_0 is the heat source.

Where nf is hybrid nanofluid, ρ_{nf} is effective density, $(\rho c_p)_{nf}$ is heat capacity, μ_{nf} is dynamic viscosity, k_{nf} is thermal conductivity, σ_{nf} is electrical conductivity which is given by[25]

$\rho_{nf} = \left((1 - \emptyset_1)\rho_f + \emptyset_1 \rho_1\right)(1 - \emptyset_2) + \emptyset_2 \rho_2$

$(\rho c_p)_{nf} = \left((\rho c_p)_f (1 - \emptyset_1) + (\rho c_p)_1 \emptyset_1\right)(1 - \emptyset_2) + (\rho c_p)_2 \emptyset_2$

$$\mu_{nf} = \frac{\mu_f}{(1-\emptyset_2)^{2.5}} \tag{7}$$

Where $\emptyset_1$ and $\emptyset_2$ are the volume fraction of gold and copper particles.

$$k_{nf} = \left(\frac{k_2 + (m-1)k_3 - (k_3 - k_2)\emptyset_2(m-1)}{k_3(m-1) + k_2 + \emptyset_2(k_3 - k_2)}\right)k_3$$

$$k_3 = (\frac{k_1 + k_f\,(m-1) - (k_f - k_1)(m-1)\emptyset_1}{k_1 + \emptyset_1(k_f - k_1) + k_f\,(m-1)}k_f$$

$$\sigma_{nf} = \sigma_3\left(\frac{\sigma_2(1+2\emptyset_2) + 2(1-\emptyset_2)\,\sigma_3}{\sigma_3(2+\emptyset_2) + \sigma_2(1-\emptyset_2)}\right)$$

$$\sigma_3 = \sigma_f\left(\frac{\sigma_1(1+2\emptyset_1) + 2\sigma_f(1-\emptyset_1)}{\sigma_1(1-\emptyset_1) + \sigma_f(2+\emptyset_1)}\right) \tag{8}$$

And in the above equation m represent the shape of factor of the proposed nanoparticles respectively; the physical characteristics of nanoparticles are classified in the Table (1).

Table 1: based on fluid and nanoparticles properties[26]

Properties	Based fluid	NPs (Gold Au)	NPs (Copper Cu)
ρ density	$\rho_f = 1050$	$\rho_1 = 19300$	$\boldsymbol{\rho_2 = 8933}$
C_p heat capcity	$C_{pf} = 3617$	$C_{p1} = 129$	$\boldsymbol{C_{p2} = 385}$
K thermal conductivity	k_f=0.52	$k_1 = 318$	$\boldsymbol{k_2 = 401}$
σ electrical conductivity	$\sigma_f = 1.33$	$\sigma_1 = 4.1 * (10^7)$	$\boldsymbol{\sigma_2 = 5.96 * (10^7)}$

For unsteady 2-D flows $\bar{V} = [U(X,Y,t), V(X,Y,t), 0]$, where U denotes the velocity component in coordinate X and V are denoted the velocity component in coordinate Y.

The following transformations are used to convert all equations in our study from fixed to the movable frame $(\bar{x}, \bar{y})$ which defines

$$X = x + ct, \qquad Y = y, \quad U = u + c, \quad V = v \tag{9}$$

Where u and v are the velocity components, presenting the dimensionless quantities which are used to find the non-dimensional analysis as

$$\left.\begin{aligned}
&\bar{x} = \frac{x}{\lambda}, \quad \bar{y} = \frac{y}{d_0}, \quad \bar{u} = \frac{u}{c}, \quad \bar{v} = \frac{v}{c}, \quad \bar{p} = \frac{d_0^2 p}{c\lambda\mu_f}, \quad \delta = \frac{d_0}{\lambda}, \quad \bar{H}_x = \frac{H_x}{H_0} \\
&\bar{H}_y = \frac{H_y}{H_0}, \bar{\eta} = \frac{\eta}{d_0^2}, \quad \theta = \frac{T - T_u}{T_l - T_u}, \qquad R_e = \frac{\rho_f c d_0}{\mu_f}, \quad R_m = \sigma_f \mu_e c d_0, \\
&S^2 = \frac{M^2}{R_e R_m}, M = H_0 d_0 \sqrt{\frac{\sigma_f}{\mu_f}}, \; P_r = \frac{\mu_f (c_p)_f}{k_f}, \; E_c = \frac{c^2}{(c_p)_f (T_l - T_u)}, \\
&R_d = \frac{4\sigma_f^* (T_l - T_u)^3}{3k_f^* k_f}, \beta = \frac{Q_0 d_0^2}{k_f (T_l - T_u)}, \bar{\psi} = c d_0 \psi, \bar{\phi} = \frac{\phi}{H_0 d_0}, \bar{E} = -\frac{E}{c H_0 \mu_e} \\
&A_1 = \frac{\rho_{nf}}{\rho_f}, \; A_2 = \frac{\mu_{nf}}{\mu_f}, \; A_3 = \frac{\sigma_{nf}}{\sigma_f}, \; A_4 = \frac{k_{nf}}{k_f}, \; A_5 = \frac{(\rho c_p)_{nf}}{(\rho c_p)_f}, \; a = \frac{d_1}{d_0} \\
&\xi_1(x) = \frac{h_1(X,t)}{d_0}, \; \xi_2(x) = \frac{h_2(X,t)}{d_0}, \; \epsilon_1 = \frac{a_1}{d_0}, \; \epsilon_2 = \frac{b_1}{d_0}
\end{aligned}\right\} \tag{10}$$

in the preceding expressions, T_u, T_l, $\bar{\psi}$, δ, η, R_e, E_c, P_r, M, R_m, β, S , $\bar{\phi}$, $\theta$and E are the upper temperature of the wall , lower temperature of the wall, the stream function, wave number, permeability parameter, the Reynolds number, the Eckert number, the Prandtl number, the Hartmann number, the magnetic Reynolds number, the internal heat generation, the magnetic force number (Stommer's number), the magnetic force function, the temperature, and the electric field in the non-dimensional form, respectively.

We introduce the dimensionless of the magnetic force function ϕ and the stream function ψ as follows:

$$u = \frac{\partial \psi}{\partial y}, \qquad v = -\delta \frac{\partial \psi}{\partial x}, \quad H_x = \frac{\partial \phi}{\partial y}, \quad H_y = -\delta \frac{\partial \phi}{\partial x}$$

After eliminating that, the continuity equation is identically satisfied and we get:

$$A_1 Re\ \delta\left(\psi_y \psi_{xy} - \psi_x \psi_{yy}\right) = -(P_m)_x + A_2 \nabla^2 \psi_y + S^2 Re\left(\delta \phi_y \phi_{xy} - \delta \phi_x \phi_{yy} + \phi_{yy}\right) - \frac{A_2}{\eta}\left(\psi_y + 1\right) \quad (11)$$

$$A_1 Re \delta^3\left(\psi_y \psi_{xx} - \psi_x \psi_{yy}\right) = (P_m)_y + A_2\, \delta^2 \nabla^2 \psi_x + S^2 Re \delta^2\left(\delta \phi_y \phi_{xx} - \delta \phi_x \phi_{xy} + \phi_{xy}\right) - \frac{A_2}{\eta} \delta^2 \psi_x \quad (12)$$

$$E = (\psi_y - \delta\left(\psi_y \phi_x - \psi_x \phi_y\right) + \frac{1}{A_3 R_m.} \nabla^2 \phi \quad (13)$$

$$\mathrm{A_5} Re\ P_r \delta\left(\psi_y \theta_x - \psi_x \theta_y\right) = A_4 \nabla^2 \theta + A_2\, E_c\ P_r \left(4\delta^2 \psi_{xy}^2 + \left(\psi_{yy} - \delta^2 \psi_{xx}\right)^2\right) + R_d (\theta^4)_{yy} + \beta \quad (14)$$

Eliminating P_m from the first and the second equations in Eq (11) and Eq (12), we obtain:

$$\mathrm{A_1} Re\ \delta\left(\psi_y \nabla^2 \psi_x - \psi_x \nabla^2 \psi_y\right) = \mathrm{A_2} \nabla^4 \psi + S^2 Re\left(\delta \phi_y \nabla^2 \phi_x - \delta \phi_x \nabla^2 \phi_y + \nabla^2 \phi_y\right) - \frac{\mathrm{A_2}}{\eta}\left(\psi_{yy} + \delta^2 \psi_{xx}\right) \quad (15)$$

For the wall dimensional stream, temperature functions and the magnetic force in the wave frame, the boundary conditions for non-conductive elastic walls are :

$$\psi = 0, \quad \phi_y = 0, \quad \psi_{yy} = 0, \qquad at \quad y = \xi_2(x)$$

$$\phi = 0, \qquad \psi_y = -1, \qquad \theta = 0, \qquad \psi = \frac{q}{2} \quad at \quad y = \xi_1(x)$$

$$\theta = 1 \quad at \quad y = \xi_2(x) \quad (16)$$

Where q represents the mean of flow rate and the peristaltic wall's non-dimensional surface are:

$$\xi_1(x) = 1 + \epsilon_1 \cos[2\pi x], \qquad \xi_2(x) = -a - \epsilon_1 \cos\left[\frac{2\pi}{\lambda}(X - Ct) + \vartheta^*\right]$$

3-Solution to the problem:

Using the Adomian decomposition method (ADM)[27-29], the exact solution to Eqs.(13), (14) and (15) is determined which is the non-linear differential equations. The linear operator is as follows:

$$L_{iy}(*) = \frac{\partial^m (*)}{\partial y^m}, \; L_{iy}^{-1}(*) = \underbrace{\int_0^y (*) dy}_{m-times}, i = 1,2,3, \ldots$$

Also, ADM contains dividing unknown functions$\Psi(x,y)$, $\theta(x,y)$ and $\phi(x,y)$ to the equations that are expressed into a sum of infinity numbers that is described in the following decomposing series:

$$\psi(\mathrm{x,y}) = \sum_{\mathrm{m=0}}^{\infty} \psi_{\mathrm{m}}(\mathrm{x,y}),\ \phi(\mathrm{x,y}) = \sum_{\mathrm{m=0}}^{\infty} \phi_{\mathrm{m}}(\mathrm{x,y}), \quad \theta(\mathrm{x,y}) = \sum_{\mathrm{m=0}}^{\infty} \theta_{\mathrm{m}}(\mathrm{x,y}), \quad (17)$$

Where $(m \geq 0)$, find the components$(\psi_0, \psi_1, \dots, \psi_m)$, $(\phi_0, \phi_1, \dots, \phi_m)$ and $(\theta_0, \theta_1, \dots, \theta_m)$ individually. By obtaining a relation that contains simple integrals, we solve for $(L_{1y}(\psi))$, As a result, the other linear operator in the system of partial differential equations is simply R1operators as follows:

$$L_{1y}(\psi) + R_1 + N_1 = f_1(x, y) \tag{18}$$

Where L_{iy} represents the highest order derivative with respect to y, i=1,2,3,…, and N_1 represents the nonlinear terms. Therefore,

$$L_{1y}(\psi) = f_1(x, y) - R_1 - N_1 \tag{19}$$

$$L_{1y}^{-1}(L_{1y}(\psi)) = L_{1y}^{-1}(f_1(x, y)) - L_{1y}^{-1}(R_1) - L_{1y}^{-1}(N_1) \tag{20}$$

We obtain: $L_{1y}^{-1}(L_{1y}(\psi)) = \psi - \sum_{j=0}^{m-1} \frac{A_j(x)y^j}{j!}$

Where$A_j(x)$ represent the integration constants which can be determined from specified conditions

$$\psi(x, y) = L_{1y}^{-1}(f_1(x, y)) - L_{1y}^{-1}(R_1) - L_{1y}^{-1}(N_1) \; + \; \sum_{j=0}^{m-1} \frac{A_j(x)y^j}{j!} \tag{21}$$

In the same form of this methodology, we get $\phi and\, \theta$,the partial differential equations solution according to suggest methodology is given as (17), the nonlinear term Ni may be represented by the infinite series of Adomain polynomials which is given in the form

$$N_i = \sum_{m=0}^{\infty} A_m \, (\phi_0, \phi_1, \dots, \phi_m, \theta_0, \theta_1, \dots, \theta_m, \Psi_0, \Psi_1, \dots, \Psi_m)$$

Where A_m represents the Adominan polynomials for the specific non–linearity that can by using the following expression:

$A_m = \frac{1}{m!}\frac{d^m}{d\xi}\left(N_i\left(\sum_{i=0}^{m} \xi^i F_i\right)\right)\Big|_{\xi=0}$, $m \geq 0$, Where F_i are component of the nonlinear terms

Using ADM to resolve the nonlinear system of equations (13)-(14) and (15) with the corresponding boundary condition (16), yields the zeros and the first order systems, we have the solution as follows:

$$\psi_0 = \frac{1}{4(\xi_1[x] - \xi_2[x])^3}(y - \xi_2[x])(-qy^2 + 2\xi_1[x]^3 + 3\xi_1[x]^2(q - 2\xi_2[x]) + 2y(q + y)\xi_2[x] + 2(q - 2y)\xi_2[x]^2 - 2\xi_1[x](y^2 + (3q - 2y)\xi_2[x] - 2\xi_2[x]^2))$$

$$\psi_1 = \mathrm{C}_1 + \mathrm{yC}_2 + \mathrm{y}^2\mathrm{C}_3 + \mathrm{y}^3\mathrm{C}_4 + (\frac{1}{5}qy^5A_2\xi_1[x]^6 + \frac{2}{5}y^5A_2\xi_1[x]^7 - \frac{6}{5}qy^5A_2\xi_1[x]^5\xi_2[x] - qy^4A_2\xi_1[x]^6\xi_2[x] - \frac{14}{5}y^5A_2\xi_1[x]^6\xi_2[x] - 2y^4A_2\xi_1[x]^7\xi_2[x] + \cdots + 144\eta A_2\xi_1[x]\xi_2[x]^8 - 16\eta A_2\xi_2[x]^9)$$

$$\phi_0 = \frac{1}{2}(-\mathrm{E\ RmA}_3\xi_1[\mathrm{x}]^2 + 2\mathrm{E\ RmA}_3\xi_1[\mathrm{x}]\xi_2[\mathrm{x}]) + \mathrm{y}(-\mathrm{E\ Rm\ A}_3\xi_2[\mathrm{x}]) + \frac{1}{2}\mathrm{E\ Rm\ y}^2\mathrm{A}_3.$$

$$\phi_1 = \mathrm{C}_5 + \mathrm{yC}_6 - \frac{1}{480\eta(\xi_1[\mathrm{x}] - \xi_2[\mathrm{x}])^4}\mathrm{ERm}^2\mathrm{y}^2\delta\mathrm{A}_3^2(5\xi_1[\mathrm{x}]^8 - 40\xi_1[\mathrm{x}]^7\xi_2[\mathrm{x}] - 5\xi_1[\mathrm{x}]^6(\mathrm{y}^2 - 4\mathrm{y}\xi_2[\mathrm{x}] - 22\xi_2[\mathrm{x}]^2) + 2\xi_1[\mathrm{x}]^5(2\mathrm{y}^3 + 60\eta + 5\mathrm{y}^2\xi_2[\mathrm{x}] - 40\mathrm{y}\xi_2[\mathrm{x}]^2 - 70\xi_2[\mathrm{x}]^3) + \cdots - 20\mathrm{Ey}\delta^2\eta\xi_2''[\mathrm{x}])) \tag{23}$$

$$\theta_0 = -\frac{(y - \xi_1[x])\left(2A_4 + \beta(y - \xi_2[x])(\xi_1[x] - \xi_2[x])\right)}{2A_4(\xi_1[x] - \xi_2[x])}.$$

$$\theta_1 = C_7 + yC_8 + (-3E_c q^2 y^4 A_2 A_4^4 p_r \xi_1[x]^4 - 12E_c q y^4 A_2 A_4^4 p_r \xi_1[x]^5 - 16R_d y^4 A_4^4 \xi_1[x]^6 - 12E_c y^4 A_2 A_4^4 p_r \xi_1[x]^6 - 32R_d y^5 \beta A_4^3 \xi_1[x]^7 + 64R_d y^3 A_4^4 \xi_1[x]^7 - 24R_d y^6 \beta^2 A_4^2 \xi_1[x]^8 + 128R_d y^4 \beta A_4^3 \xi_1[x]^8 - 96R_d y^2 A_4^4 \xi_1[x]^8 - 8R_d y^7 \beta^3 A_4 \xi_1[x]^9 + \cdots + 16A_4^5 \xi_2[x]^{10}) \quad (24)$$

The $C_1, C_2, C_3, C_4, C_5, C_6, C_7$ and C_8 are large constants cofficients can be determined by using boundary condition Eq.(16) and Mathematic software .As a result, the system approximate solution appears such as this.

$$\psi = \sum_{m=0}^{\infty} \psi_m, \theta = \sum_{m=0}^{\infty} \theta_m, \phi = \sum_{m=0}^{\infty} \phi_m \quad (25)$$

The gradient of magnetic pressure is obtain from Eq (25) to Eq.s (11-12), we get:

$$(P_m)_x = A_1 Re\, \delta(\psi_y \psi_{xy} - \psi_x \psi_{yy}) + A_2 \nabla^2 \psi_y + S^2 Re(\delta \phi_y \phi_{xy} - \delta \phi_x \phi_{yy} + \phi_{yy}) - \frac{A_2}{\eta}(\psi_y + 1)$$

$$(P_m)_y = A_1 Re \delta^3(\psi_y \psi_{xx} - \psi_x \psi_{yy}) - A_2\, \delta^2 \nabla^2 \psi_x - S^2 Re \delta^2(\delta \phi_y \phi_{xx} - \delta \phi_x \phi_{xy} + \phi_{xy}) + \frac{A_2}{\eta} \delta^2 \psi_x \quad (26)$$

The non- dimensional current density is obtained through:

$$J = -\nabla^2 \phi \quad (27)$$

So, the electric field E is obtained from

$$E = \psi_y - \delta(\psi_y \phi_x - \psi_x \phi_y) + \frac{1}{A_3 R_m.} \nabla^2 \phi \quad (28)$$

4-Discusses the results:

This part aims to look at the examination of the graphical results of several physical parameters that are used in the proposed modelling. We have drawn the graphics below, in particular: streamlines, axial and normal velocity, current density, magnetic force contours, and temperature profile. To make it more meaningful, we looked at many cases, including wavenumber δ, magnetic Reynolds number Rm, permeability parameter η, electric field parameter E, high and low Reynolds number Re, and Hartmann number M. The numerical values were chosen based on the previous literature[30, 31] and the trapping for flow is discussed graphically, all figures are plotted by using the Mathematica program.

4.1Trapping phenomenon:

Trapping is a peristaltic pumping mechanism, in which a streamlined flow forms a circular path, which is called a bolus at the volumetric flow rate value. In order to examine the effects of the Reynolds number Re and the phase difference ϑ^* in an asymmetric channel, Figures (2 - 3) were drawn. It is observed from Figure (2) that the increasing values of Re, always has a minor influence negligible at the size of de trapped bolus, one can clearly see that in a graphic streamline. It is displayed in Figure 3 which illustrates the effect of phase difference ϑ^* on trapping. It can be observed that the bolus that appears in the central region for ϑ^*=0 travels to the left and gradually decreases in the size as ϑ^* increases. The effect of the wave number δ and permeability parameters η on trapping are observed in Figures (4-5). In Figure (4), we noticed that when the wavenumber δ rises, the trapped bolus of the asymmetric channel increases in size. We observed that the permeability parameters η reduced the number of trapped bolus when permeability parameters η values are increasing as displayed in Figure (5). It can be noted from the Figure (6) that the formation of trapped boluses increases in size with the increase of Rm number.

Figures (7 to 9) develop magnetic force outlines to show how major physical parameters are considered. The contour of the magnetic force happens in parallel with the flow field. In Figure

(7), it has been noted that the contours of the magnetic force rapidly increase with the magnetic Reynolds number Rm. The values of Rm rise indicate more credible magnetic induction. Additionally, it demonstrates that the effects of the magnetic scatter and dynamo are reduced as the magnetic Reynolds number increases. In Figure (8), it is clear that as the permeability parameters η increase, the number of magnetic contours reduces and the size of the bolus changes.

In Figure (9), it is developed to show the behavior of magnetic Reynolds number Rm on trapping phenomena, it is seen that the raise of the wavenumber parameter enhances the magnetic force contours in both upper and lower half of the channel.

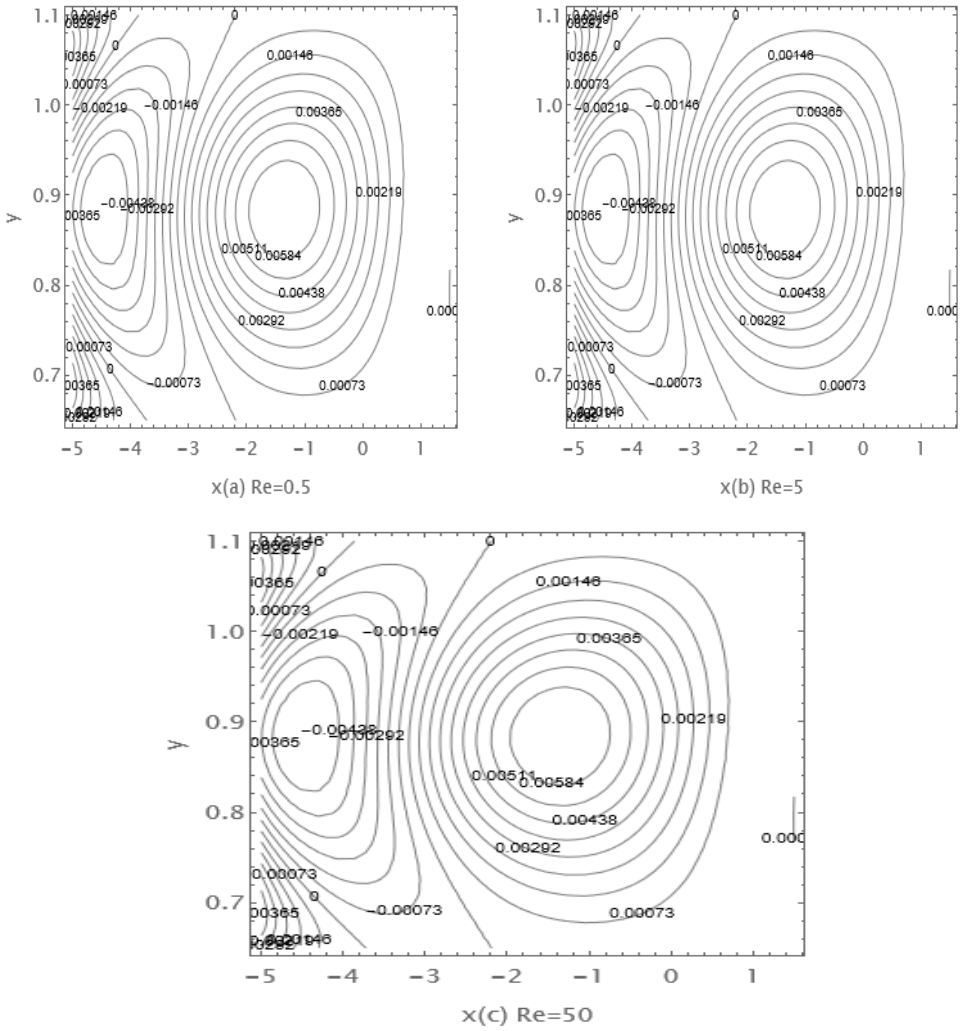

Figure 2: Impact of Reynolds number on the stream lines ($\epsilon_1 = 0.2, \epsilon_2 = 1.2, \mathrm{Rm} = 0, M = 1, q = 0.1, E = 0.5\,,\ \delta = 0.2, \emptyset_1 = 0.05, \emptyset_2 = 0.1, \eta = 0.2, \vartheta^* = \frac{\pi}{4}, a = 2$)

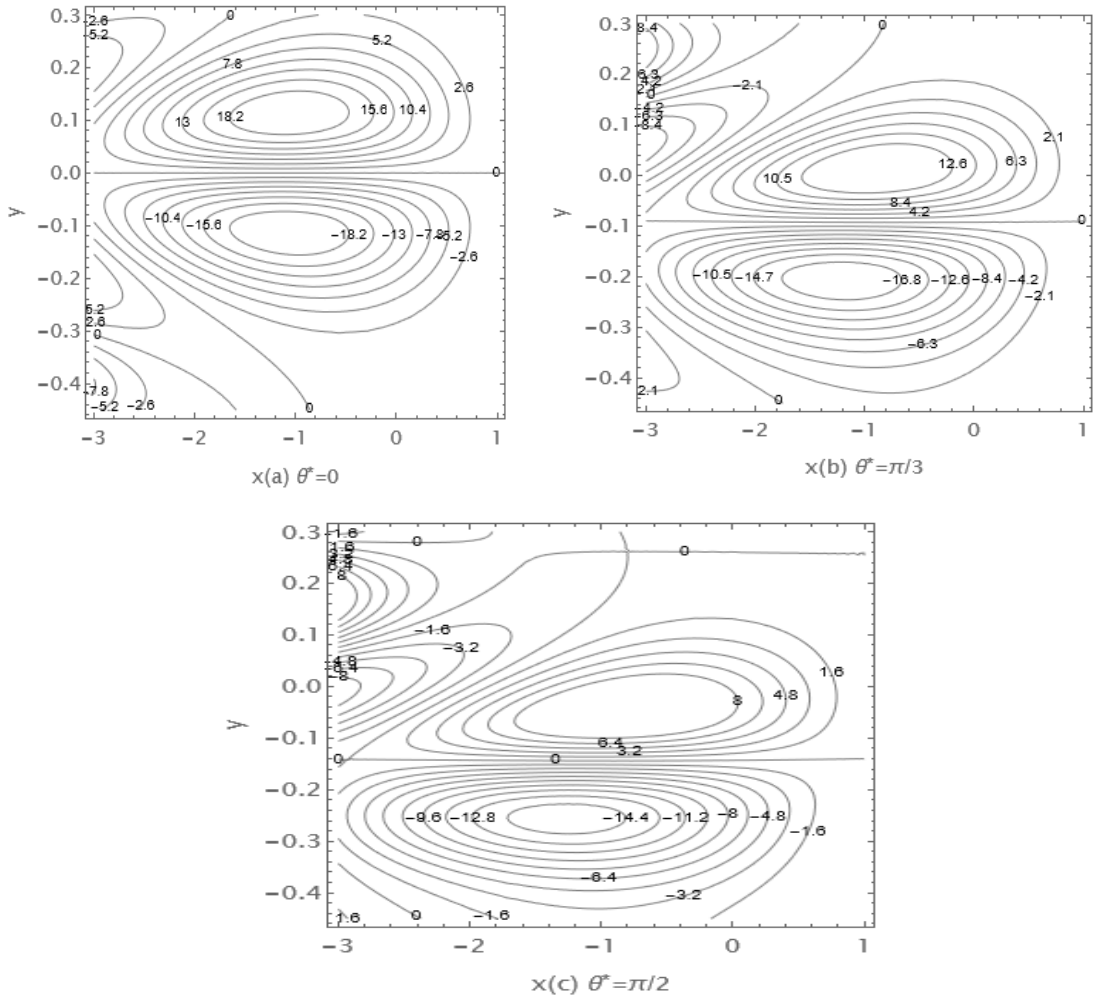

Figure 3: Impact of phase difference ϑ^*on the stream lines($\epsilon_1 = 0.2, \epsilon_2 = 1.2, \mathrm{Re} = 0.5, \mathrm{Rm} = 0.5, M = 1, q = 0.3, E = 0.5, \delta = 0.2, \emptyset_1 = 0.05, \emptyset_2 = 0.1, \eta = 0.2, \vartheta^* = \frac{\pi}{4}, a = 2$)

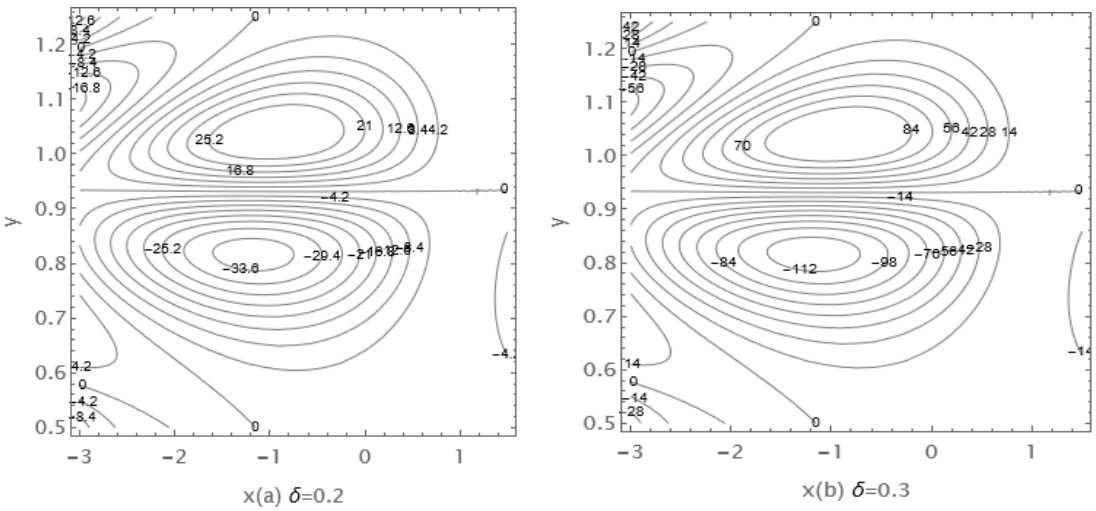

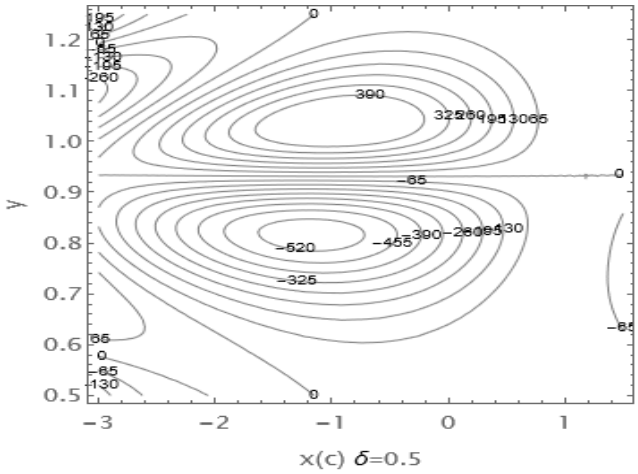

Figure 4: Impact of wave number on the stream lines ($\epsilon_1 = 0.2, \epsilon_2 = 1.2, \mathrm{Re} = 0.1, \mathrm{Rm} = 0.1, M = 3, q = 0.5, E = 0.5\ , \emptyset_1 = 0.05, \emptyset_2 = 0.1, \eta = 0.2, \vartheta^* = \frac{\pi}{4}, a = 2$)

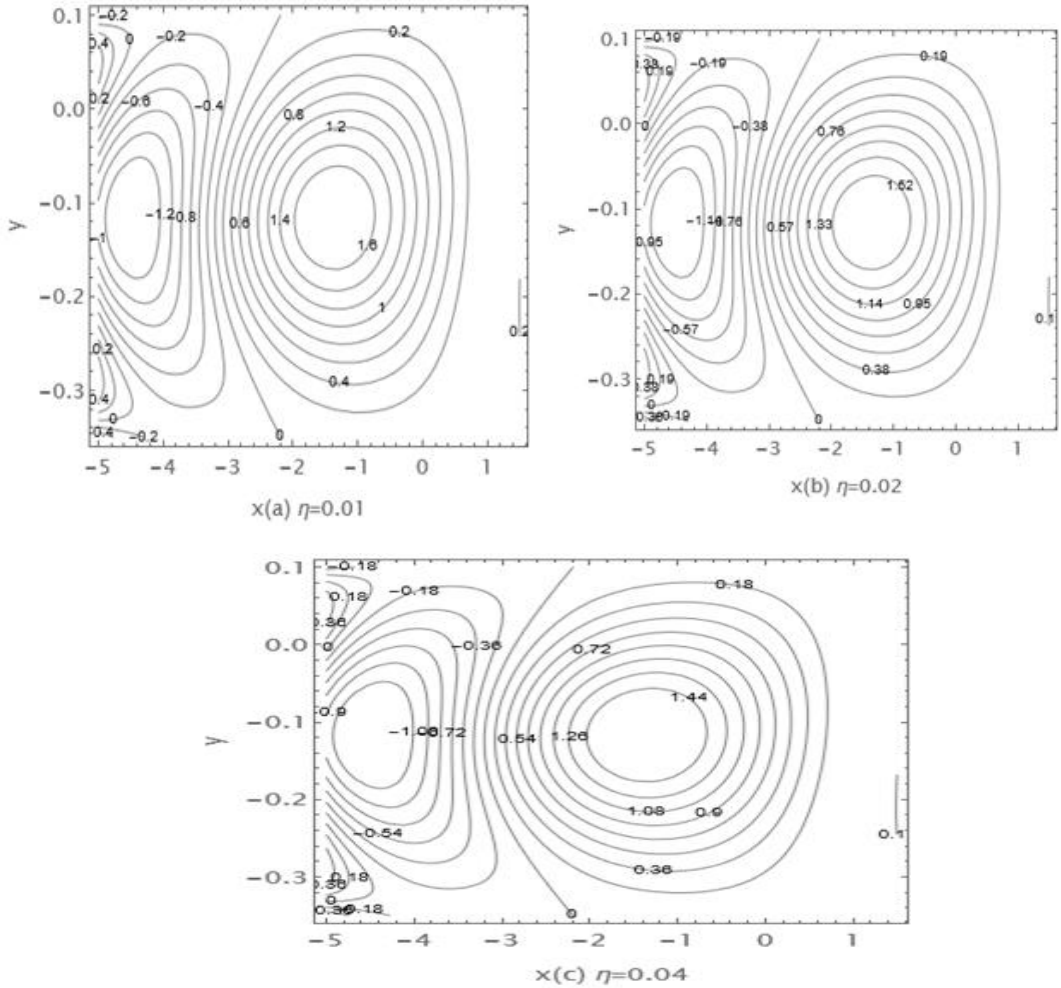

Figure 5: Impact of permeability parameters η on the stream lines ($\epsilon_1 = 0.2, \epsilon_2 = 1.2, Re = 0.1, Rm = 0, M = 0.005,\ q = 0.1, E = 0.5, \delta = 0.2, \emptyset_1 = 0.05, \emptyset_2 = 0.1, \vartheta^* = \frac{\pi}{4}, a = 2$)

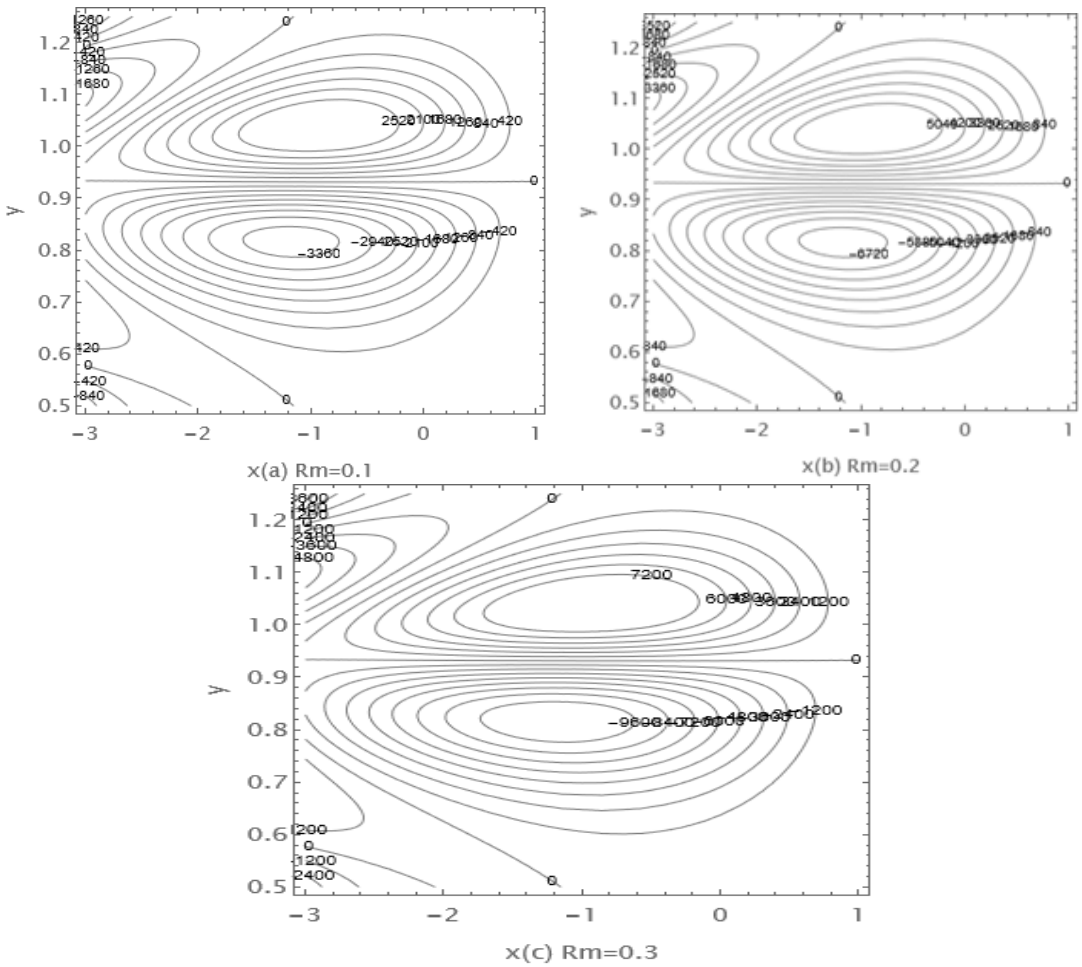

Figure 6: Impact of Rm on the stream lines ($\epsilon_1 = 0.2, \epsilon_2 = 1.2, E = 0.3,$ Re $= 0.1,$ Rm $= 0.1, M = 30, q = 0.5,$

$$\delta = 0.2, \emptyset_2 = 0.1, \eta = 0.2, \emptyset_1 = 0.05, \vartheta^* = \frac{\pi}{4}, a = 2)$$

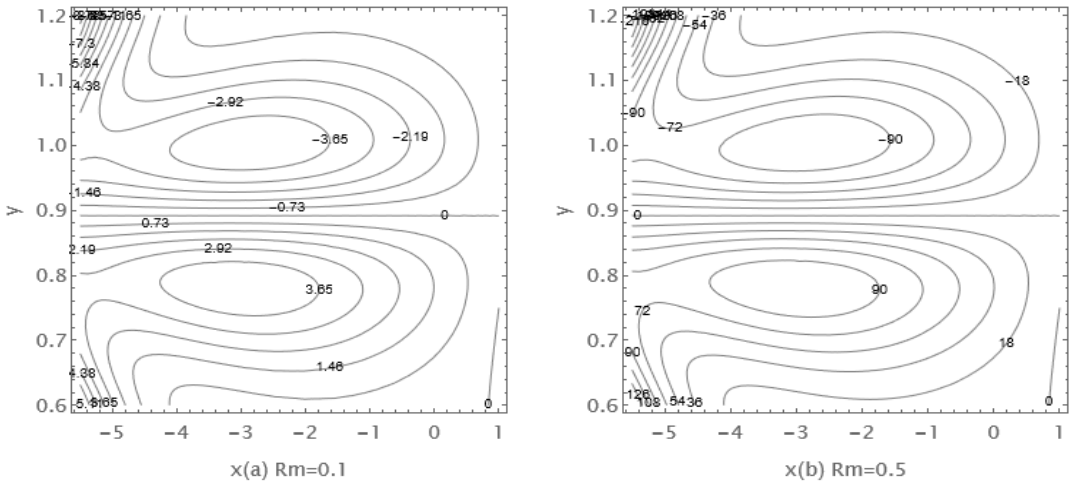

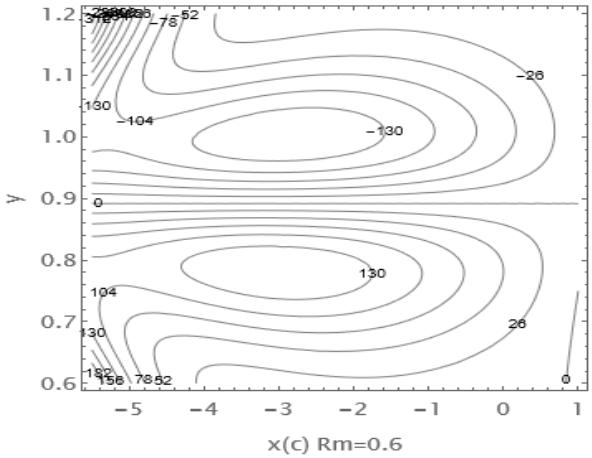

Figure 7: Impact of Rm on the magnetic force contours ($\epsilon_1 = 0.2, \epsilon_2 = 1.2, \mathrm{Re} = 0.1, M = 3, \vartheta^* = \frac{\pi}{4}, E = 0.5,$
$q = 0.1, \delta = 0.2, \emptyset_1 = 0.05, \emptyset_2 = 0.1, \eta = 0.2, a = 2$)

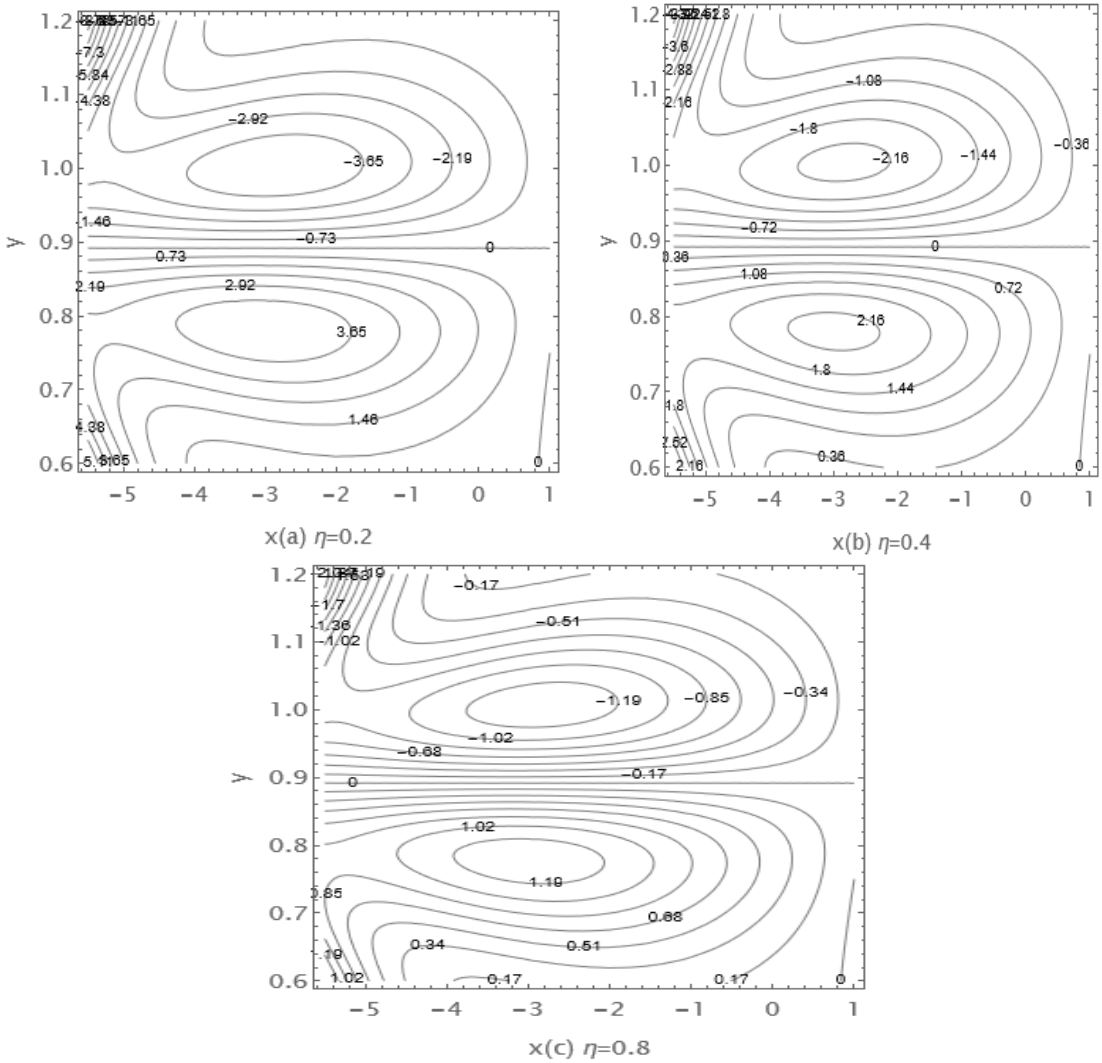

Figurer 8: Impact of permeability parameters η on the magnetic force contours ($\epsilon_1 = 0.2, \epsilon_2 = 1.2, \mathrm{Re} = 0.1,$
$\mathrm{Rm} = 0.1, M = 3, q = 0.1, E = 0.5, \delta = 0.2, \emptyset_1 = 0.05, \emptyset_2 = 0.1, \eta = 0.2, \vartheta^* = \frac{\pi}{4}, a = 2$)

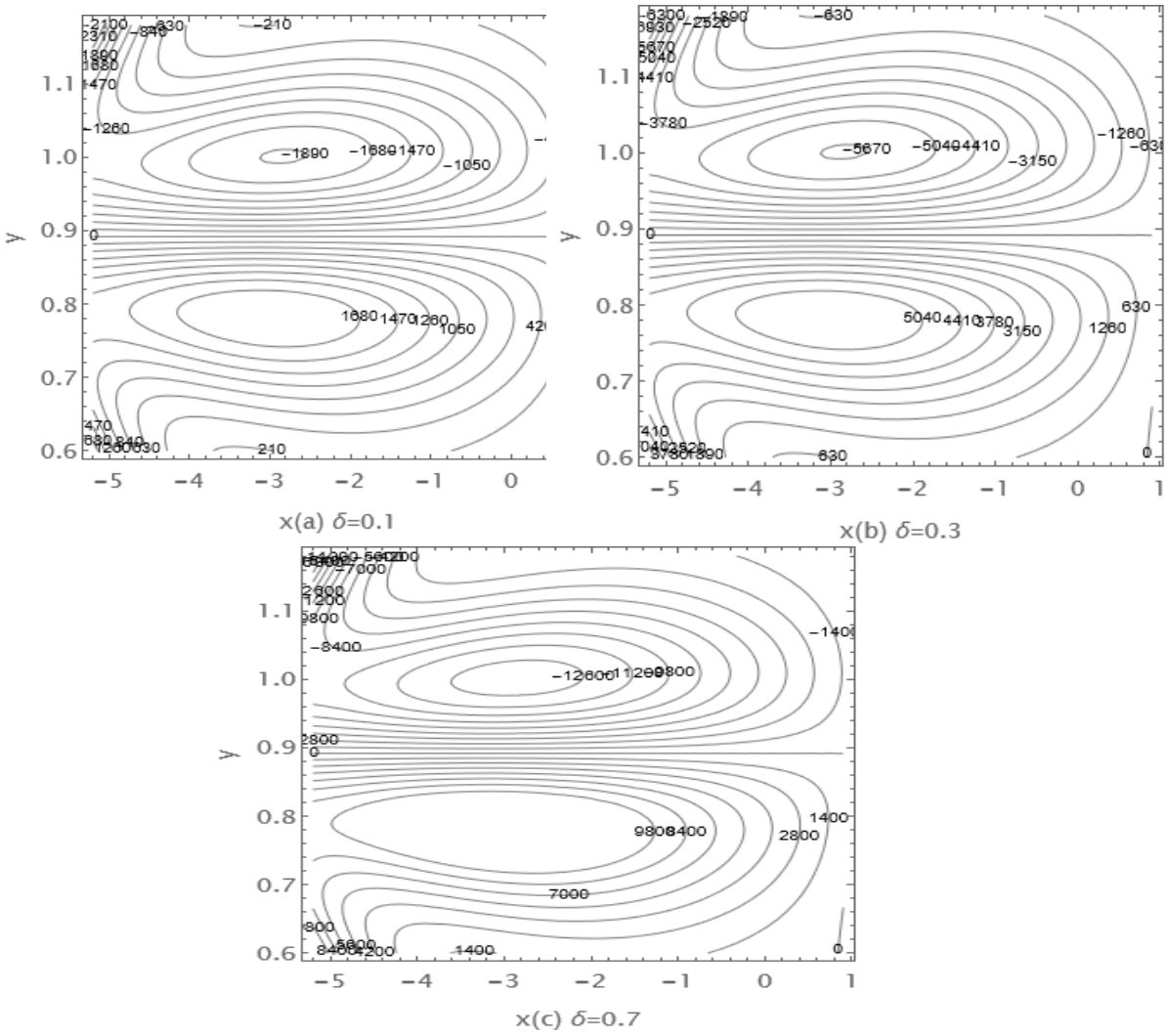

Figure 9: Impact of wavenumber on the magnetic force contours($\epsilon_1 = 0.2, \epsilon_2 = 1.2, \vartheta^* = \frac{\pi}{4}$, Re = 0.1 , Rm = 3, $M = 6, q = 0.1, E = 0.5, \emptyset_1 = 0.05, \emptyset_2 = 0.1, \eta = 0.2, a = 2$)

4.2 Velocity profile:

This subsection describes an examination of velocity distribution. Graphics have been drawn to show the evolution of the velocity profile. The impact of different values of major parameters on the axial velocity u is explained in Figure (10). The effects of magnetic Reynolds number Rm, wave numbers δ on the axial velocity profile can be observed in Figure (10 (a-b)). It can be noticed that the axial velocity increases in the region $y < -0.5$. Otherwise, it decreases as Rm and δ increase. The influence of the Hartmann number M on the axial velocity is displayed in Figure (10c) an enhancement of axial velocity which is examined due to the higher M. The fluid axial velocity is shown in Figure (10d) to be at its highest when there is gold nanofluid present. However, it reduces for base fluid, then further for hybrid nanofluid, and it finally becomes the lowest for copper nanofluid.

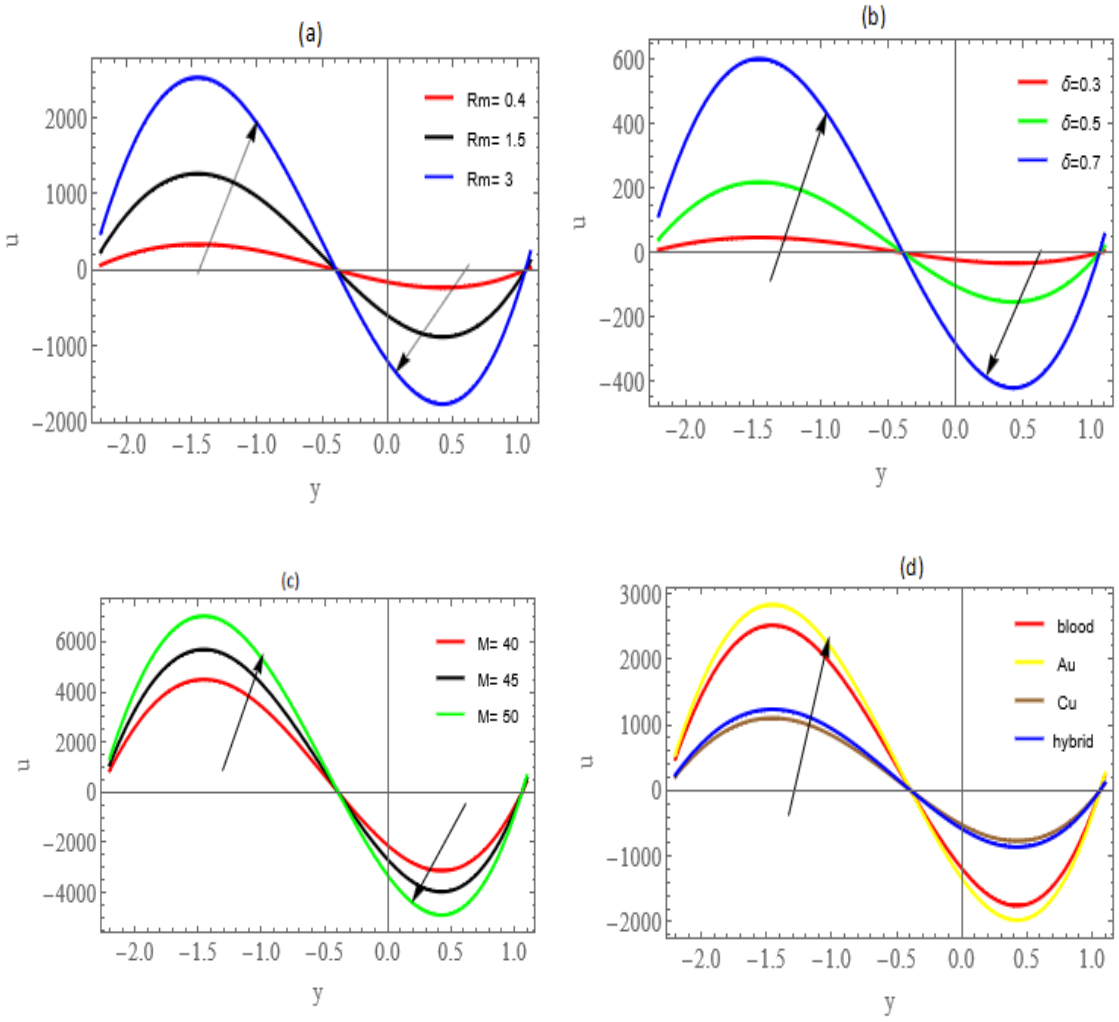

Figure 10: Axial velocity with the different physical parameters$x = 0.2, \epsilon_1 = 0.2, \epsilon_2 = 1.2, \vartheta^* = \frac{\pi}{4}, a = 2, q = 0.5(\boldsymbol{a})(\mathrm{Re} = 0.1, M = 30, E = 0.3, \delta = 0.2, \emptyset_1 = 0.05, , \emptyset_2 = 0.1, \eta = 0.2)(\mathbf{b})(\mathrm{Re} = 0.1, \mathrm{Rm} = 6, M = 0.5, q = 0.5, E = 0.3, \emptyset_1 = 0.05, \emptyset_2 = 0.1, \eta = 0.2)(\mathbf{c})(\mathrm{Re} = 50, \mathrm{Rm} = 3, q = 0.5, E = 0.3, \delta = 0.2, \emptyset_1 = 0.05, , \emptyset_2 = 0.1, \eta = 0.2)(\boldsymbol{d})(\mathrm{Re} = 50, \mathrm{Rm} = 20, M = 0.5, q = 0.5, E = 0.3, \delta = 0.3, \eta = 0.2)$

Figure 11 shows the behavior of parameters involved in normal velocity. The effect of different values of major parameters on the normal velocity is explained. In Figure (11a), it can be observed that the normal velocity of the fluid is similar to the axial velocity within region $y > -0.5$. Figures (11b-11c) illustrate the behavior of magnetic Reynolds number Rm and wave number on the normal velocity component v. We notice that the normal velocity decreases with Rm and δ in the region $-2.2 \leq y \leq -0.5$, and it increases in the region$-0.5 \leq y \leq 1$. The impact of the Hartmann M on normal velocity is displayed in Figure (11d) an enhancement of normal velocity is examined due to the increase of M.

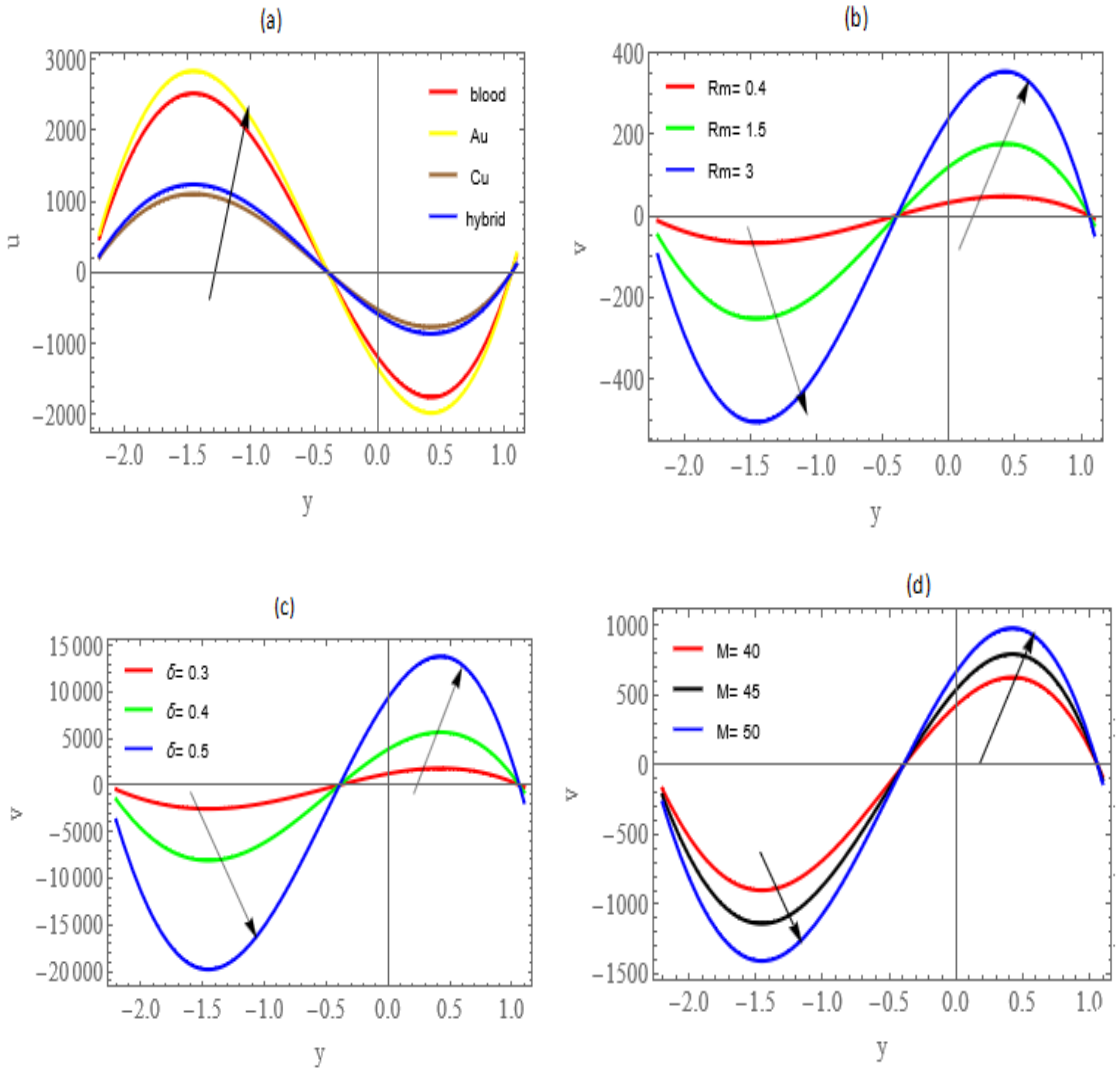

Figure11 normal velocity with the different physical parameters parameters $x = 0.2, \epsilon_1 = 0.2,\ \epsilon_2 = 1.2, \vartheta^* = \frac{\pi}{4}, a = 2, q = 0.5$ **(a)**$(\mathrm{Re} = 50, \mathrm{Rm} = 20, M = 0.5, E = 0.3, \delta = 0.3, \eta = 0.2)$**(b)**$(\mathrm{Re} = 50, M = 30, q = 0.5, E = 0.3, \delta = 0.2, , \emptyset_1 = 0.05, \emptyset_2 = 0.1, \eta = 0.2)$**(c)**$(\mathrm{Re} = 0.1, \mathrm{Rm} = 3, M = 3, E = 0.5, , \emptyset_1 = 0.05, , \emptyset_2 = 0.1, \eta = 0.2)$**(*d*)**$(\mathrm{Re} = 50, \mathrm{Rm} = 3, E = 0.3, \delta = 0.2, , \emptyset_1 = 0.05, , \emptyset_2 = 0.1, \eta = 0.2)$

4.3- Magnetic force and Current density profile:

The influence of important physical parameters on magnetic force ϕ and current density J profile are sketched in Figure (12) and Figure (13).

Magnetic force ϕ and current density J profile for the gold nanofluids in Figure (12a-13a) are higher than those for the hybrid nanofluid and base fluids. They are also higher than those for copper nanofluids. In Figure (12(b-c)), the conduct of current density profile J is depicted for wavenumber δ, and magnetic Reynolds number Rm, it is seen that the current density J rises in the central area of the channel when Rm and δ are increased. While an opposite behavior is observed closed to the channel walls, and the magnetic force rises by increasing Rm and δ as shown in Figure(13(b-c)). The influence of permeability parameters η on the profile of current

density J is shown in Figure(12d), and it can be seen that J decreases as η increases close to the channel center. We observe how the impact of η on the magnetic force ϕ in Figure(13d). It has been found that the magnetic force rises at the channel's center, and it slowly declines near the channel's walls as η increases.

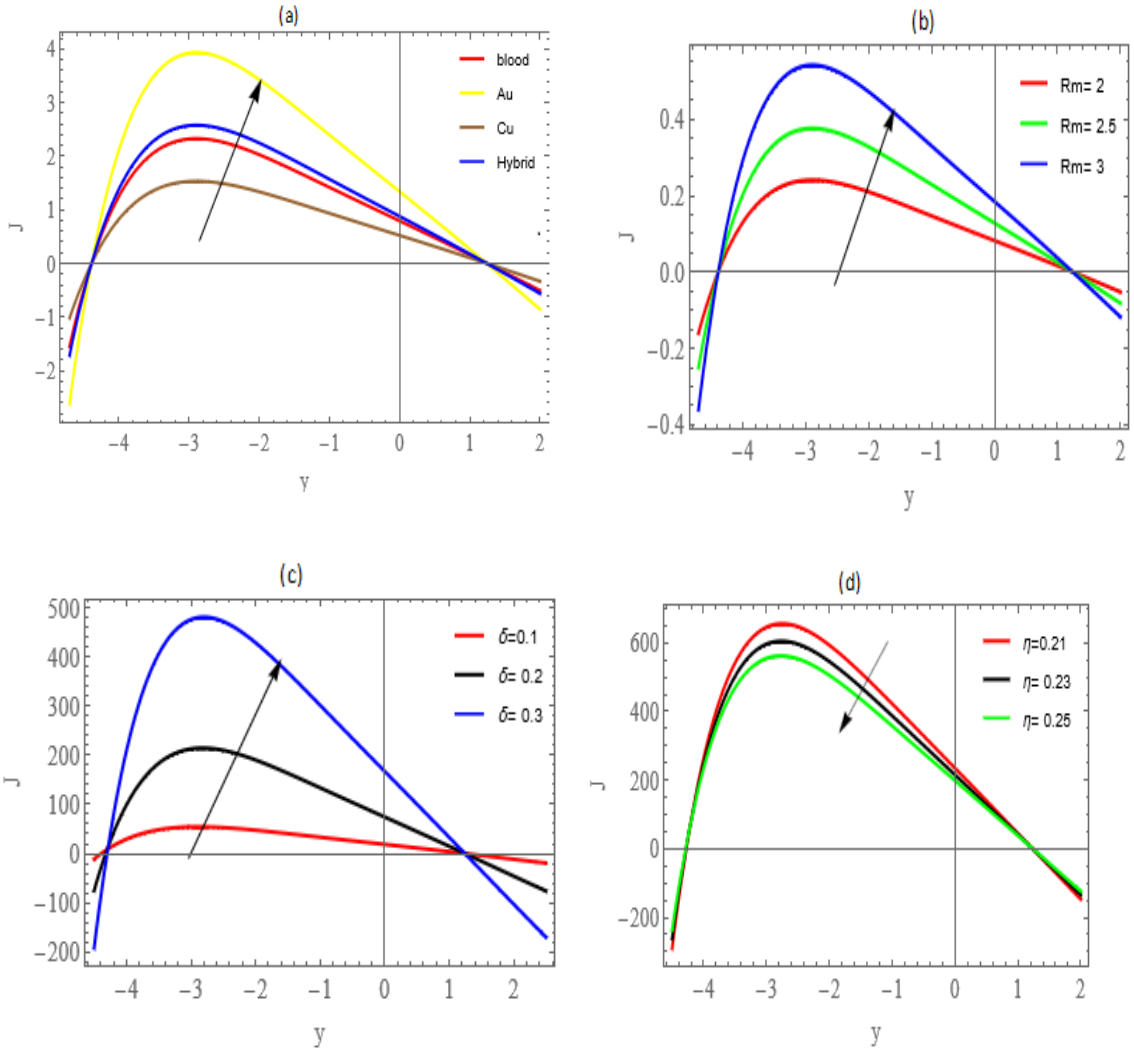

Figure 12: Current density profile with the various physical parameters $x = 0.2, \epsilon_1 = 0.2,\ \epsilon_2 = 1.2, \vartheta^* = \frac{\pi}{4}, a = 2, q = 0.5(\boldsymbol{a})(\mathrm{Re} = 0.5, \mathrm{Rm} = 6, M = 0.3, E = 0.3, \delta = 0.1, \eta = 0.3)\mathbf{b})(\ \mathrm{Re} = 0.6, \mathrm{Rm} = 2, M = 0.3, E = 0.3, \delta = 0.1, \emptyset_1 = 0.1, \emptyset_2 = 0.15, \eta = 0.3)\mathbf{(c)}(\ \mathrm{Re} = 0.5, \mathrm{Rm} = 30, M = 0.3, E = 3, \emptyset_1 = 0.05, \emptyset_2 = 0.1, \eta = 0.3)(\mathbf{d})(\mathrm{Re} = 0.5, \mathrm{Rm} = 30, M = 0.3, E = 0.3, \delta = 0.3, \emptyset_1 = 0.05, \emptyset_2 = 0.1)$

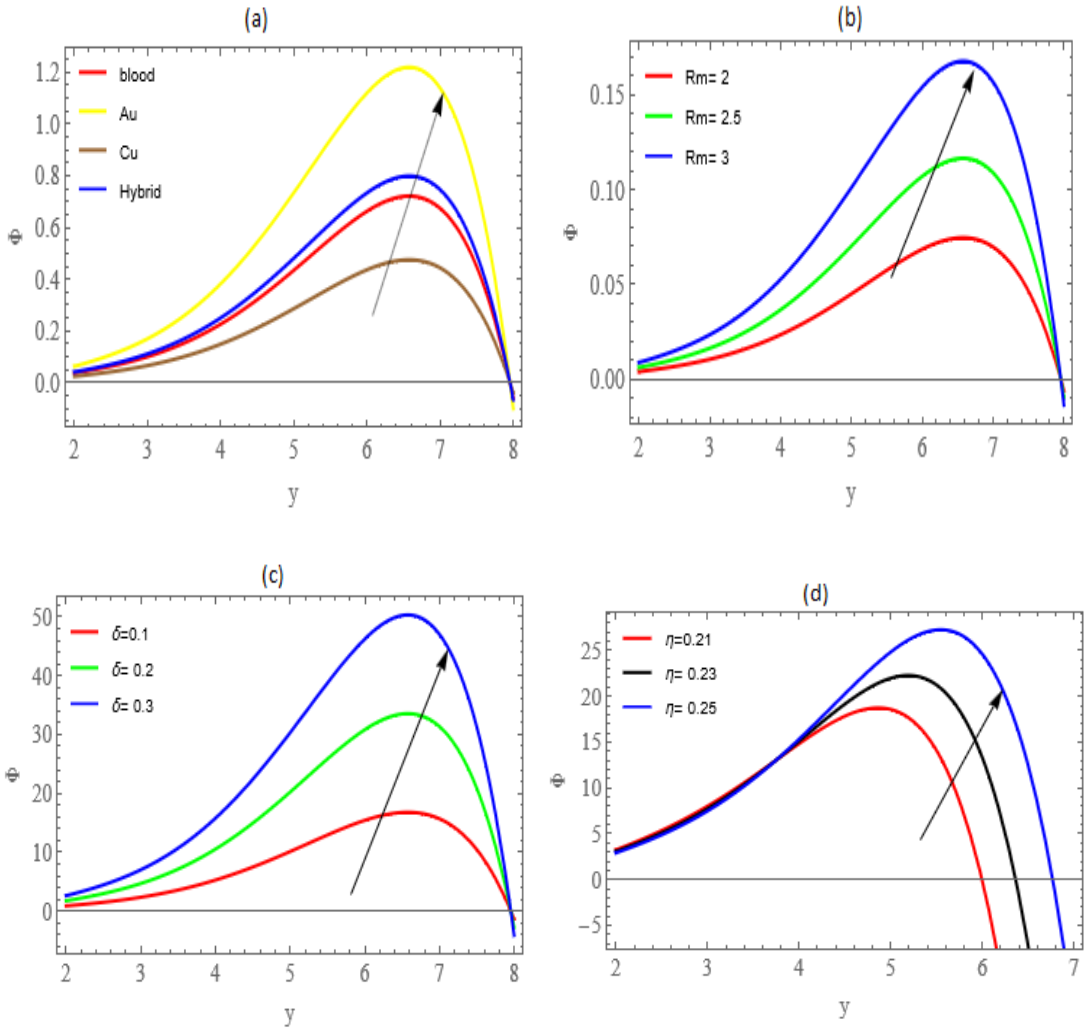

Figure13: Magnetic force profile with the various physical parameters $x = 0.2, \epsilon_1 = 0.2,\ \epsilon_2 = 1.2, \vartheta^* = \frac{\pi}{4}, a = 2, q = 0.5(\boldsymbol{a})(\mathrm{Re} = 0.5, \mathrm{Rm} = 6, M = 0.3, E = 0.3, \delta = 0.1, \eta = 0.3)\mathbf{(b)}(\ \mathrm{Re} = 0.6, \mathrm{Rm} = 2, M = 0.3, E = 0.3, \delta = 0.1, \emptyset_1 = 0, \emptyset_2 = 0.15, \eta = 0.3)\mathbf{(c)}(\ \mathrm{Re} = 0.5, \mathrm{Rm} = 30, M = 0.3, E = 3, \phi_1 = 0.05, \emptyset_2 = 0.1, \eta = 0.3)(\mathbf{d})(\mathrm{Re} = 0.5, \mathrm{Rm} = 30, M = 0.3, E = 0.3, \delta = 0.3, \emptyset_1 = 0.05, \emptyset_2 = 0.1)$

4.4-Temperature profile:

This subsection examines the effect of the different major physical parameters on the temperature profile in Figure (14). The results indicate the nearly parabolic nature of the temperature profiles. Figure (14a) shows the influence of heat radiation Rd on the temperature profile. The findings show that there exists a considerable increase in the temperature of the fluid for the increasing value of the thermal radiation Rd. An increase in radiation parameters tends to improve the spread of electromagnetic waves and thermal conduction decreases. Afterward, it has an intense impact on thermal diffusion at the speed. Since heat transfer diffusion occurs due to random molecular motion, the adjacent molecules move less vigorously and transport less energy between them when they are extinguished. The influence of the Prandtl number p_r is shown in Figure (14b) this indicates that p_r greater results in an improvement of the temperature profile. In Figure (14(c)), a decline in the temperature profile is noticed as the heat absorption β increase. Consequently, an improvement of the temperature is observed toward rising values of E_c as shown in Figure (14d).

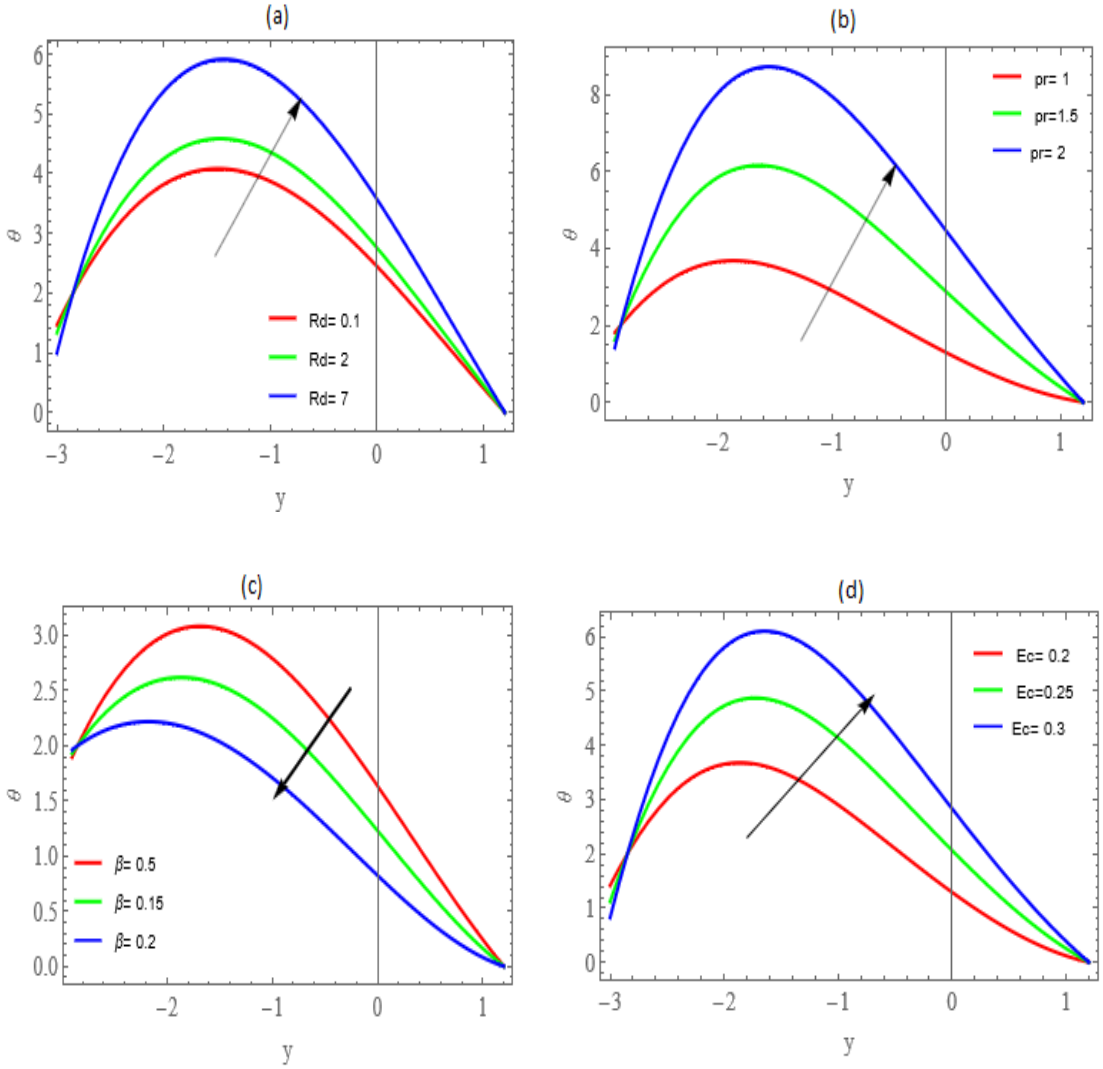

Figure 14: Temperature profile with the different physical parameters$x = 1, \epsilon_1 = 0.2, \epsilon_2 = 1.2, \emptyset_1 = 0.1, \emptyset_2 = 0.1, a = 2, , \vartheta^* = \frac{\pi}{4}$,**(a)** $(p_r = 3, \delta = 0.5, \mathrm{Re} = 0.5, q = 0.5, \eta = 0.2, \mathrm{Rm} = 5, M = 0.5, \beta = 0, \mathrm{Ec} = 0, E = 0.5)$**(b)**$(\delta = 0.5, \mathrm{Re} = 0.5, q = 0.5, \eta = 0.2, \mathrm{Rd} = 0.5, \mathrm{Rm} = 5, M = 0.5, \beta = 0.5, \mathrm{Ec} = 0.2, E = 0.5)$**(c)** $(p_r = 3, \delta = 0.5, \mathrm{Re} = 0.5, q = 0.5, \mathrm{Rd} = 0.1, \mathrm{Rm} = 5, M = 0.5, \eta = 0.2, \mathrm{Ec} = 0, E = 0.5$**(d)** $(p_r = 1, \delta = 0.5, \mathrm{Re} = 0.5, q = 0.5, \eta = 0.2, \mathrm{Rd} = 0.5, \mathrm{Rm} = 5, M = 0.5, \beta = 0.5, E = 0.5)$

5-Conclusion:

The peristaltic transport of nonlinear thermal radiation and magnetic force on hybrid bio-nanofluid are examined through a porous medium for an asymmetric channel in the effect of a high and a low Reynolds number with applying a magnetic field. The governing equations representing momentum, Maxwell, and heat equations are considered. Utilizing the Adomian decomposition technique, exact solutions for axial velocity, normal velocity, current density, stream function, temperature, and magnetic force have been presented. Below is a summary of the study's main outcomes:

- With an increase in M improves the axial velocity field.

- The normal velocity profile exhibits split conduct in regions: y > - 0.5 and y < 0.5 with respect to all physical parameters.
- The gold nanofluid is higher than those for the hybrid and base fluids. They are higher than those for the copper nanofluid in magnetic force and current density.
- An increase in Rm and δ enhances the magnetic force and current density.
- An improvement of the temperature is observed towards increasing values of Ec.
- The formation of trapped boluses increases in size with the increase of Rm number.
- An increase in η the number, the number of magnetic contours reduces and the size of the bolus changes.

These results can be used to support how PET scan influences blood flow within the human body, particularly when gold, copper, or both nanoparticles are combined to treat blood cancers.

References:

[1] S. U. Choi and J. A. Eastman, "Enhancing thermal conductivity of fluids with nanoparticles," Argonne National Lab.(ANL), Argonne, IL (United States)1995.

[2] P. B. A. Reddy, "Biomedical aspects of entropy generation on electromagnetohydrodynamic blood flow of hybrid nanofluid with nonlinear thermal radiation and non-uniform heat source/sink," *The European Physical Journal Plus*, vol. 135, pp. 1-30, 2020.

[3] H. S. Chahregh and S. Dinarvand, "TiO2-Ag/blood hybrid nanofluid flow through an artery with applications of drug delivery and blood circulation in the respiratory system," *International Journal of Numerical Methods for Heat & Fluid Flow*, 2020.

[4] P. C. Chen, S. C. Mwakwari, and A. K. Oyelere, "Gold nanoparticles: from nanomedicine to nanosensing," *Nanotechnology, science and applications*, vol. 1, p. 45, 2008.

[5] S. U.-S. Choi, "Nanofluid technology: current status and future research," Argonne National Lab.(ANL), Argonne, IL (United States)1998.

[6] N. Arjunan, C. M. Singaravelu, J. Kulanthaivel, and J. Kandasamy, "A potential photocatalytic, antimicrobial and anticancer activity of chitosan-copper nanocomposite," *International journal of biological macromolecules*, vol. 104, pp. 1774-1782, 2017.

[7] Q. K. Jawad and A. M. Abdulhadi, "Influence of MHD and porous media on peristaltic transport for nanofluids in an asymmetric channel for different types of walls," *International Journal of Nonlinear Analysis and Applications*, 2022.

[8] L. Z. Hummady, I. T. Abbas, and R. A. Mohammed, "Inclined Magnetic Field of Non-uniform and Porous Medium Channel on Couple Stress Peristaltic Flow and application in medical treatment (Knee Arthritis)," *Journal of Southwest Jiaotong University*, vol. 54, 2019.

[9] M. Kothandapani and J. Prakash, "Influence of heat source, thermal radiation, and inclined magnetic field on peristaltic flow of a hyperbolic tangent nanofluid in a tapered asymmetric channel," *IEEE transactions on nanobioscience*, vol. 14, pp. 385-392, 2014.

[10] S. Noreen, M. Rashidi, and M. Qasim, "Blood flow analysis with considering nanofluid effects in vertical channel," *Applied Nanoscience*, vol. 7, pp. 193-199, 2017.

[11] M. Rashid, K. Ansar, and S. Nadeem, "Effects of induced magnetic field for peristaltic flow of Williamson fluid in a curved channel," *Physica A: Statistical Mechanics and its Applications*, vol. 553, p. 123979, 2020.

[12] G.-J. Hu, A. Bilal, A.-K. Kamel, M. Muhammad Tanseerul, K. Sami Ullah, K. M Ijaz, *et al.*, "Peristaltic activity in an asymmetric inclined channel with inertial forces under the inducement of magnetic field: finite element method," *Alexandria Engineering Journal*, 2021.

[13] L. Zhang, M. M. Bhatti, M. Marin, and K. S. Mekheimer, "Entropy analysis on the blood flow through anisotropically tapered arteries filled with magnetic zinc-oxide (ZnO) nanoparticles," *Entropy*, vol. 22, p. 1070, 2020.

[14] M. A. Murad and A. M. Abdulhadi, "Peristaltic Transport of Power-Law Fluid in an Elastic Tapered Tube with Variable Cross-Section Induced by Dilating Peristaltic Wave," *Iraqi Journal of Science*, pp. 1293-1306, 2021.

[15] A. H. Seikh, A. Akinshilo, M. Taheri, M. Rahimi-Gorji, N. Alharthi, I. Khan, *et al.*, "Influence of the nanoparticles and uniform magnetic field on the slip blood flows in arterial vessels," *Physica Scripta*, vol. 94, p. 125218, 2019.

[16] R. S. Kareem and A. M. Abdulhadi, "Impacts of Heat and Mass Transfer on Magneto Hydrodynamic Peristaltic Flow Having Temperature-dependent Properties in an Inclined Channel Through Porous Media," *Iraqi Journal of Science*, pp. 854-869, 2020.

[17] S. Das, B. Barman, and R. Jana, "Influence of Hall and Ion-Slip Currents on Peristaltic Transport of Magneto-Nanofluid in an Asymmetric Channel," *BioNanoScience*, vol. 11, pp. 720-738, 2021.

[18] R. Abo-Elkhair, M. Bhatti, and K. S. Mekheimer, "Magnetic force effects on peristaltic transport of hybrid bio-nanofluid (AuCu nanoparticles) with moderate Reynolds number: An expanding horizon," *International Communications in Heat and Mass Transfer*, vol. 123, p. 105228, 2021.

[19] N. Manjunatha and R. Sumithra, "Non-Darcian-Bènard Double Diffusive Magneto-Marangoni Convection in a Two Layer System with Constant Heat Source/Sink," *Iraqi Journal of Science*, pp. 4039-4055, 2021.

[20] N. Manjunatha and R. Sumithra, "Effects of heat source/sink on Darcian-Benard-Magneto-Marangoni convective instability in a composite layer subjected to nonuniform temperature gradients," 2022.

[21] N. Manjunatha, R. Sumithra, and R. Vanishree, "Darcy-Benard double diffusive Marangoni convection in a composite layer system with constant heat source along with non uniform temperature gradients," *Malaysian Journal of Fundamental and Applied Sciences*, vol. 17, pp. 7-15, 2021.

[22] A. K. Hage and L. Z. Hummady, "Influence of inclined magnetic field and heat transfer on peristaltic transfer Powell-Eyring fluid in asymmetric channel and porous medium," *International Journal of Nonlinear Analysis and Applications*, vol. 13, pp. 631-642, 2022.

[23] R. S. Kareem and A. M. Abdulhadi, "Effect of MHD and Porous Media on Nanofluid Flow with Heat Transfer: Numerical Treatment," *Journal of advanced research in fluid mechanics and thermal sciences*, vol. 63, pp. 317-328, 2019.

[24] A. W. Salih and S. B. Habeeb, "Peristaltic Flow with Nanofluid under Effects of Heat Source, and Inclined Magnetic Field in the Tapered Asymmetric Channel through a Porous Medium," *Iraqi Journal of Science*, pp. 4445-4459, 2022.

[25] J. Akram, N. S. Akbar, and D. Tripathi, "Blood-based graphene oxide nanofluid flow through capillary in the presence of electromagnetic fields: A Sutterby fluid model," *Microvascular Research*, vol. 132, p. 104062, 2020.

[26] D. Tripathi, J. Prakash, A. K. Tiwari, and R. Ellahi, "Thermal, microrotation, electromagnetic field and nanoparticle shape effects on Cu-CuO/blood flow in microvascular vessels," *Microvascular Research*, vol. 132, p. 104065, 2020.

[27] H. O. Bakodah and A. Ebaid, "The Adomian decomposition method for the slip flow and heat transfer of nanofluids over a stretching/shrinking sheet," *Rom. Rep. Phys*, vol. 70, p. 115, 2018.

[28] M. M. Bhatti, M. Marin, A. Zeeshan, and S. I. Abdelsalam, "Recent trends in computational fluid dynamics," *Frontiers in Physics*, vol. 8, p. 593111, 2020.

[29] G. Shit, N. Ranjit, and A. Sinha, "Adomian decomposition method for magnetohydrodynamic flow of blood induced by peristaltic waves," *Journal of Mechanics in Medicine and Biology*, vol. 17, p. 1750007, 2017.

[30] M. Raza, R. Ellahi, S. M. Sait, M. Sarafraz, M. S. Shadloo, and I. Waheed, "Enhancement of heat transfer in peristaltic flow in a permeable channel under induced magnetic field using different CNTs," *Journal of Thermal Analysis and Calorimetry*, vol. 140, pp. 1277-1291, 2020.

[31] K. S. Mekheimer, N. Saleem, T. Hayat, and A. Hendi, "Simultaneous effects of induced magnetic field and heat and mass transfer on the peristaltic motion of second-order fluid in a channel," *International journal for numerical methods in fluids*, vol. 70, pp. 342-358, 2012.